Observation of Large Low-Field Magnetoresistance in Spinel Cobaltite: A New Half-Metal

Peng Li[1][†],*, Chuan Xia[2][†], Dongxing Zheng[1], Ping Wang,[1] Chao Jin[1], and Haili Bai[1]

Dr. Peng Li, Dr. Dongxing Zheng, Dr. Ping Wang, Dr. Chao Jin and Prof. Haili Bai
Tianjin Key Laboratory of Low Dimensional Materials Physics and Preparing Technology,
Institute of Advanced Materials Physics, Faculty of Science, Tianjin University, Tianjin
300072, People's Republic of China
E-mail: (pengli@tju.edu.cn)

Dr. Chuan Xia
Division of Physical Science and Engineering, King Abdullah University of Science and
Technology (KAUST), Thuwal 23955, Kingdom of Saudi Arabia

Low-field magnetoresistance is an effective and energy-saving way to use half-metallic
materials in magnetic reading heads and magnetic random access memory. Common spin-
polarized materials with low field magnetoresistance effect are perovskite-type manganese,
cobalt, and molybdenum oxides. In this study, we report a new type of spinel cobaltite
materials, self-assembled nanocrystalline $NiCo_2O_4$, which shows large low field
magnetoresistance as large as -19.1% at 0.5 T and -50% at 9 T (2 K). The large low field
magnetoresistance is attributed to the fast magnetization rotation of the core nanocrystals. The
surface spin-glass is responsible for the observed weak saturation of magnetoresistance under
high fields. Our calculation demonstrates that the half-metallicity of $NiCo_2O_4$ comes from the
hopping e_g electrons within the tetrahedral Co-atoms and the octahedral Ni-atoms. The
discovery of large low-field magnetoresistance in simple spinel oxide $NiCo_2O_4$, a non-
perovskite oxide, leads to an extended family of low-field magnetoresistance materials.

1. Introduction

The magnetoresistance (MR) effect of ferromagnets has attracted considerable attention because it can be used in spintronic (spin transport electronics) applications, including magnetic reading heads, magnetic sensors, spin-valves and magnetic random access memory devices.[1] To optimize and maximize the MR ratio, the carriers in ferromagnets should be spin-polarized or - in other words - half-metal.[2] In most half-metals, however, a large magnetic field is required to generate large MR. For example, magnetic fields of several tesla are required to suppress the thermal magnetic disorder and obtain the colossal magnetoresistance of doped manganite. In half metallic spinel Fe_3O_4 the MR is linearly proportional to the magnetic field, indicating a moderate MR ratio (about -10% to -20%) at very high magnetic fields.[3] To advance their use in commercial applications, much research has been devoted to study the low field magnetoresistance (LFMR) in several spin-polarized nanocrystalline materials.[4, 5] Spin-polarized materials are mainly perovskite-type manganese,[5, 6] cobalt,[7] and molybdenum oxides.[8] Compared to the widely investigated perovskite, half-metallic spinel oxide has some outstanding characteristics such as its relative abundance and also its high Curie temperature. The latter is typically 860 K for Fe_3O_4.[9] On the other hand, both the poor conductivity at low temperature and small LFMR of nanocrystalline Fe_3O_4 (-10% at 200 K) limits its performance in practical applications.[10] Hence, there is strong motivation to search for large LFMR in spinel oxides. Unlike the widely investigated iron-based spinel oxides, cobalt-based spinel oxides are rarely studied in spintronics. The spinel cobaltite, ferrimagnetic ordered $(Co^{3+})_A[Ni^{2+}Co^{3+}]_BO_4$ is an unusual mixed-valence oxide in which Ni^{2+} occupy the octahedral (B) sites and Co^{3+} are distributed across both octahedral and tetrahedral (A) sites with a lattice constant of 8.114 Å.[11] Because of its superior conductivity (epitaxial film: ρ_{300K}=800 μΩcm),[12] spinel $NiCo_2O_4$ has potential uses in various areas and commercial applications like electrocatalytic activity,[13] water electrolysis,[14] negative electrodes of lithium-ion batteries,[15] photodetectors and transparent

2

conducting oxides.[16, 17] Compared to the excellent and well-known ability to store energy electrochemically,[18] the magnetotransport property of $NiCo_2O_4$ in spintronics is yet to be studied and exploited. In our study, we found a large LFMR of -20% at 0.5 T and -50% at 9 T in self-assembled nanocrystalline $NiCo_2O_4$, a non-perovskite system. We also demonstrate the feasibility of multifunctional spinel oxide $NiCo_2O_4$ to be used in spintronic applications, thereby adding a new member to the family of LFMR materials.

2. Results and Discussion

The X-ray diffraction (XRD) pattern of as-synthesized $NiCo_2O_4$ is shown in **Figure 1**a. All diffraction peaks are consistent with the standard $NiCo_2O_4$ spinel structure without secondary phases. The stoichiometry of cations is confirmed by energy dispersive spectroscopy in connection with a scanning electron microscope (SEM) and transmission electron microscope (TEM). The crystal structure is shown in Figure 1b. Based on the strongest diffraction peak (311) the calculated lattice constant for $NiCo_2O_4$ is 8.11 Å, which is consistent with the literature value. The full width at half maximum (FWHM) of the peaks for the as-synthesized $NiCo_2O_4$ was broad, suggesting that the samples were nanocrystalline in nature. The average grain size of the nanocrystalline areas is 10.2 nm. This was estimated from the FWHM (0.81°) of the strongest peak (311) and the empirical Scherrer formula $d = 0.9\lambda / (\beta \cos\theta)$, in which β and θ are the FWHM (in radian) and Bragg angle, respectively. The SEM image illustrates that as-synthesized $NiCo_2O_4$ nanopowders maintain a uniform urchin-like morphology with nanocrystalline self-assembled nanotubes growing radially from the center – see Figure 1c. The corresponding TEM image (Figure 1d) shows that $NiCo_2O_4$ nanotubes consist of several nanocrystals of about 10 nm size, which is in agreement with our XRD results. The high resolution TEM image in Figure 1e reveals that the lattice plane distances are 2.86 Å and 2.01 Å. They fit well into the (220) and (400) interplanar spaces in $NiCo_2O_4$. The lattice fringes with different orientations suggest that the

3

as-synthesized $NiCo_2O_4$ is polycrystalline in nature. This is further confirmed by the corresponding selected area electron diffraction pattern (Figure 1f).

Figure 2a shows the temperature-dependent magnetization of nanocrystalline $NiCo_2O_4$ measured by zero-field-cooling (ZFC) and field-cooling (FC) under a magnetic field of 10 Oe. We find the following features: (i) The ZFC curve reaches its maximum at the average blocking temperature, T_B, of 137 K and then decreases rapidly; (ii) The ZFC and FC curves show reversibility above 230 K. Both features demonstrate the superparamagnetism of nanocrystalline $NiCo_2O_4$ at high temperatures and a particle size distribution around 10 nm. According to a "building block" of 10 nm grain size, the magnetic anisotropic constant K of $NiCo_2O_4$ is estimated:[19, 20]

$$K = \frac{\ln(\tau_m / \tau_0)k_B T_B}{<V>} \approx \frac{25 k_B T_B}{<V>} . \tag{1}$$

Here τ_m is the characteristic measurement time of SQUID-VSM (~10 s), and τ_0 is closely related to the natural frequency of precession ($10^{-9} \sim 10^{-13}$), k_B and $<V>$ refer to the Boltzmann constant and nanoparticle volume, respectively. The factor 25 is the commonly used $\ln(\tau_m / \tau_0)$-value in conventional magnetometry.[19, 21] Using Equation 1, the magnetic anisotropic constant K of $NiCo_2O_4$ is calculated as 9.02×10^5 erg/cm^3. This is consistent with the literature value for monodispersive $NiCo_2O_4$ nanoparticles.[22] The magnetic hysteresis loops at different temperatures are shown in Figure 2b. At high magnetic fields all loops show weak saturation. As the temperature decreases, the superparamagnetism becomes ferromagnetism reaching a magnetic moment of 1.54 μB/f.u. (34.69 emu/g) at H=5 T and T=2 K. A value of 2.0 μB/f.u. has been reported previously.[11] The small deviation from the literature value may be explained by the nanocrystalline morphology in our sample. Surface spin-glass usually forms at the surface or boundary of nanocrystals. To check whether surface spin-glass is present or not, the imaginary (out-of-phase, χ'') parts of the AC susceptibility of nanocrystalline $NiCo_2O_4$ was measured as a function of temperature with an AC driving field

with a 4 Oe amplitude. The data were collected during heating from 2 to 300 K after the ZFC

process - see Figure 3b. The temperature for the maximum (T_P) shifts towards higher values

when the frequency increases. This suggests the presence of reentrant spin-glass and a low-

temperature disordered frozen magnetic state at the grain surfaces. In order to better

understand the surface spin-glass state, temperature-dependent ZFC and FC magnetization at

different magnetic fields was performed (Figure 2d). The blocking temperature in the ZFC

curve shifts toward lower temperatures for higher magnetic fields. In addition, bifurcation

between ZFC and FC magnetization can still be observed even when the magnetic field

exceeds 1 T. This is indicative of the incomplete elimination of a surface spin-glass state with

a magnetic field as high as 5 T.

Figure 3a displays the resistance and magnetoresistance ratio of $NiCo_2O_4$ as a function

of the magnetic field at 2 K. The MR ratio is defined as $MR = (\rho_H - \rho_{max}) / \rho_{max} \times 100$, where

ρ_{max} and ρ_H are the resistivity at coercive and applied magnetic fields, respectively. The

clear LFMR shows a butterfly shape and reaches -19.1% at 0.5 T and -25.3% at 1.0 T in self-

assembled $NiCo_2O_4$. The presence of large LFMR probably suggests that $NiCo_2O_4$ is a half-

metal. The MR saturates at high fields, leading to a MR ratio of -50% at 9.0 T. The magnetic

moments in both the nanoparticle bulk and surface spin-glass could cause the observed LFMR

and weak saturation of MR at high magnetic fields. We find that by increasing the

temperature the LFMR decreases gradually (Figure 3b). In epitaxial $NiCo_2O_4$ films the MR is

negligible (-2% at 1 T).[12] To better understand the LFMR we measured the temperature

dependent resistivity of $NiCo_2O_4$. Figure 3c and 3d show resistivity as a function of $T^{-1/2}$ and

$T^{-1/4}$. In a single crystal $NiCo_2O_4$ nanoplate it is possible that variable range hopping

(VRH, $\rho \propto T^{-1/4}$) dominates below 100 K while both VRH and nearest-neighbour hopping

(NNH, $\rho \propto T^{-1}$) contribute at temperatures above 100 K.[17] In our nanocrystalline $NiCo_2O_4$,

VRH dominates in the high temperature region (T>100 K). In the low temperature region, the linear relation of ρ and $T^{-1/2}$ indicates intergrain tunnelling. [23]

For the purpose of uncovering the physical origin of LFMR in nanocrystalline $NiCo_2O_4$, we annealed $NiCo_2O_4$ and investigated its MR. To maintain the nanocrystalline morphology of $NiCo_2O_4$, the annealing temperature is kept at 350 °C. $NiCo_2O_4$ is not stable for temperatures above 400 °C (Supplementary Information, Figure S1). The crystallinity and morphology remain nearly unchanged after annealing at 350 °C for 4 h, 8 h and 12 h (Supplementary Information, Figure S2 and S3). Figure 4a gives the 2 K MR of annealed $NiCo_2O_4$ for different annealing times. The MR at 2 K decreases from -50% in as-synthesized sample to -37% (4 h), -35% (8 h) and -29% (12 h) after annealing. The MR ratio of $NiCo_2O_4$ shows the same temperature dependent behaviour, - see inset in **Figure 4**a (field-dependent MR is shown in Supplementary Information, Figure S4). As shown in Figure 4b, the resistivity of annealed $NiCo_2O_4$ is reduced greatly compared to the as-synthesized sample (Figure 3c and 3d). Given nearly identical size of the nanocrystals, the reduced resistivity can be attributed to the better connectivity of the nanocrystals. Although the transport mechanism conforms with intergrain tunnelling at low temperatures and VRH at high temperatures, in the annealed samples the low temperature region of intergrain tunneling ($\rho \propto T^{-1/2}$) is greatly reduced - see Figure 4b and its inset. Improved conductivity and non-ideal intergrain tunnelling can explain the decreased LFMR in the annealed samples. To better understand its MR behaviour, the ZFC and FC magnetization curves of annealed samples under a magnetic field of 10 Oe are shown in Figure 4c. The blocking temperature is enhanced slightly from 137 K (as-synthesized) to 149 K (4 h), 165 K (8 h) and 170 K (12 h). This indicates a slight increase of the nanocrystalline size after annealing. This is further supported by the increase of high field magnetization ($H = 5$ T and T=2 K) from 1.54 µB/f.u (as-synthesized) to 1.68 µB/f.u (4 h), 1.78 µB/f.u (8 h) and 1.84 µB/f.u (12 h) - as shown in Figure 4d. Surface spin-

glass can also be observed in the annealed sample (Supplementary Information, Figure S5). Interestingly, compared to the as-synthesized $NiCo_2O_4$, a distinct exchange bias $H_{ex} = 42$ Oe was observed in the annealed sample (12 h) after field cooling under a strong magnetic field of 5 T – see Figure 4e. The origin of this exchange bias and its relation with MR will be discussed in the following.

The MR in magnetic granular systems can be expressed as $MR \propto \langle \cos \varphi \rangle \propto (M/M_S)^2$,[24] where φ is the angle between the directions of magnetization of two adjacent grains. To better understand the large LFMR and the magnetic behaviour in general, we compare the magnetic field dependent normalized MR and $-(M/M_S)^2$ of the as-synthesized and annealed sample (12 h) at different temperatures – see **Figure 5**. At 2 K, the normalized MR nearly coincides with $-(M/M_S)^2$ in the whole magnetic field region for both kinds of samples. Hence, we can conclude that the LFMR comes from the rotation of magnetization in the core of the nanocrystals. The slight increase of magnetization from surface spin-glass accounts for the weak saturation in MR at high fields. This is schematically shown in the inset of Figure 5a. Interestingly, the MR deviates from $-(M/M_S)^2$ significantly at 200 K for the annealed sample where the measurement temperature is higher than the blocking temperature (T_B=170 K). The vanishing LFMR and its deviation from $-(M/M_S)^2$ at temperatures higher than T_B are ascribed to the fast flip of spin moments by thermal agitation. In addition, the MR of the annealed sample is near linearly proportional to the magnetic field at 200 K. This characteristic is similar to the small and linear field-dependence as well as the relative small negative MR in half-metallic Fe_3O_4 films, which is attributed to strong antiferromagnetic coupling across atomic boundaries, antiphase boundaries (APBs).[3, 25] Usually, this type of cation dislocation is observed in epitaxial films during the nucleation and coalescence of islands. It is caused by the relative low crystal symmetry of spinel (*Fd*3*m*) compared to the substrates. It is the antiferromagnetic coupled

7

APBs that flip the spin of hopping electrons and decrease the spin polarization largely.[3] To

our surprise, APBs were observed in the annealed $NiCo_2O_4$ nanocrystals. Figure 4f shows

typical APBs in our annealed sample, shifting a quarter interplanar spacing along (110). On

the other hand, grain boundaries in as-synthesized samples are disordered and amorphous, as

displayed in Figure 1e. Another indication of the presence of APBs and strong

antiferromagnetic coupling is the increased negative magnetization revealed by the ZFC curve

at low temperatures as the annealing time increases (Figure 4c). In addition to non-ideal

intergrain tunnelling, the presence of APBs can cause reduced LFMR and the small exchange

bias field (Figure 4e) in annealed $NiCo_2O_4$. The formation of APBs is probably caused by the

rotation of nanocrystals during the annealing process and consistent with the oriented SAED

of a textured nanotube (Supplementary Information, Figure S6).

Because of the observed large LFMR in nanocrystalline $NiCo_2O_4$ we wanted to find out

whether it is a half-metal in nature or not. After geometric optimization with the appropriate

Hubbard correction parameters U_{eff}=1.5 (Ni) and 5.5 (Co) eV,[26] the calculated lattice

parameter is 8.152 Å which is consistent with the measured value of 8.11 Å. **Figure 6** shows

both total and partial density of states for $NiCo_2O_4$. Only spin-down e_g electrons of Ni on B

sites and Co on A sites were present at the Fermi level in $NiCo_2O_4$ with a relatively small

energy gap of ~1.3 eV for spin-up electrons near the Fermi level. This strongly suggests that

the good conductivity of $NiCo_2O_4$ can be attributed to e_g electron hopping within Ni (B sites)

and Co (A sites). Furthermore, the calculated moment is an integer and 2 μB/f.u, which

perfectly agrees with our experimental results as well as previously reported values.[11] The

calculation results indicate that $NiCo_2O_4$ is a half-metal.

3. Conclusions

In summary, a rather large LFMR was observed in self-assembled nanocrystalline

$NiCo_2O_4$ synthesized using the hydrothermal method. Superparamagnetism is observed in

$NiCo_2O_4$ nanocrystals with a blocking temperature of 137 K. The surface spin-glass was confirmed by the shifts of the χ'' peak toward higher temperature with increasing frequency and bifurcation between the ZFC and FC magnetization even as high as 5 T. A MR of -50% was observed at 2 K. We attribute the large LFMR to the fast magnetization rotation of core nanocrystals. The weak saturation of MR at high fields is attributed to the surface spin-glass. Compared to the as-synthesized sample, LFMR is reduced in annealed $NiCo_2O_4$ due to non-ideal intergrain tunnelling and the presence of APBs. The half-metallicity of $NiCo_2O_4$ was confirmed by our first-principle calculation. We demonstrated the large LFMR in simple spinel oxides $NiCo_2O_4$, a non-peroskite-type oxide adding to the family of LFMR materials.

4. Experimental Sections

Sample Fabrication: Nanostructured powders of spinel $NiCo_2O_4$ were synthesized by the hydrothermal method. Typically, 8 mmol of $Co(NO_3)_2 \cdot 6H_2O$, 4 mmol of $Ni(NO_3)_2 \cdot 6H_2O$ and 15 mmol of urea were dissolved in 80 ml deionized water to form a clear pink solution. This solution was subsequently transferred into a Teflon-lined autoclave and kept at 120 ℃ for 4 h. After cooling down to the room temperature, the resultants were obtained and washed with deionized water and ethanol. After drying, these powders were annealed at 350 ℃ for 2 h at a rate of 3 ℃ min^{-1} to acquire inverse spinel $NiCo_2O_4$.

Characterization of Structure and Physical Properties: The structure was analysed by x-ray diffraction (XRD), scanning electron microscopy (SEM) and transmission electron microscopy (TEM). The magnetic properties were measured using a magnetic property measurement system (SQUID-VSM, Quantum Design). The transport properties ewere studied through cold-hydraulically pressing self-assembly nanocrystalline $NiCo_2O_4$ into a

pellet (5×5×1 mm) at a pressure of 2.322 GPa. The magnetotransport properties were measured with a physical property measurement system (Dynacool, Quantum Design).

Calculation method: Calculations made within the framework of density function theory were performed using the Vienna Ab-initio Simulation Package.[27] The wave functions of the inner electrons consisting of orbitals up to (and including) the 3p levels for A and B as well as the 1s level for O were described by the projector augmented wave method (PAW).[28] Calculations were carried out on a spinel cubic cell containing 56 atoms (8 A and 16 B and 32 O) in the reciprocal space of the cell and computed with a Monkhorst-Pack grid of 4×4×4 k points.[29] The optimized parameters of the 56-atom highly symmetrical unit cell were Hubbard corrected (U_{eff}=5.5 (Ni) and 1.5 eV (Co)).

Supporting Information

Supporting Information is available from the Wiley Online Library or from the author.

[1]   S. Jin, M. Mccormack, T. H. Tiefel, R. Ramesh, J Appl Phys 1994, 76, 6929.
[2]   R. A. Degroot, F. M. Mueller, P. G. Vanengen, K. H. J. Buschow, Phys Rev Lett 1983, 50, 2024.

[3]   W. Eerenstein, T. T. M. Palstra, S. S. Saxena, T. Hibma, Phys Rev Lett 2002, 88, 247204.

[4]   H. Y. Hwang, S. W. Cheong, Science 1997, 278, 1607; H. Y. Hwang, S. W. Cheong, Nature 1997, 389, 942.

[5]   J. M. D. Coey, A. E. Berkowitz, L. Balcells, F. F. Putris, A. Barry, Phys Rev Lett 1998, 80, 3815.

[6]   A. P. Chen, Z. X. Bi, C. F. Tsai, J. Lee, Q. Su, X. H. Zhang, Q. X. Jia, J. L. MacManus-Driscoll, H. Y. Wang, Adv Funct Mater 2011, 21, 2423; M. Staruch, H. Y. Gao, P. X. Gao, M. Jain, Adv Funct Mater 2012, 22, 3591; J. Jeon, H. S. Alagoz, R. Boos, J. Jung, K. H. Chow, Appl Phys Lett 2014, 104, 122405; X. K. Ning, Z. J. Wang, Z. D. Zhang, Adv Funct Mater 2014, 24, 5393; A. Sadhu, S. Bhattacharyya, Chem Mater 2014, 26, 1702.

[7]   Y. Wang, H. J. Fan, Small 2012, 8, 1060.

[8]   K. L. Kobayashi, T. Kimura, H. Sawada, K. Terakura, Y. Tokura, Nature 1998, 395, 677; M. Garcia-Hernandez, J. L. Martinez, M. J. Martinez-Lope, M. T. Casais, J. A. Alonso, Phys Rev Lett 2001, 86, 2443; T. T. Fang, Phys Rev B 2005, 71, 064401; J. F. Wang, J. Zhang, B. Hu, Z. B. Gu, S. T. Zhang, J Phys D Appl Phys 2014, 47, 445003.

[9]   H. Zeng, C. T. Black, R. L. Sandstrom, P. M. Rice, C. B. Murray, S. H. Sun, Phys Rev B 2006, 73, 020402; S. Kohiki, T. Kinoshita, K. Nara, K. Akiyama-Hasegawa, M. Mitome, Acs Appl Mater Inter 2013, 5, 11584.

[10]   Z. L. Lu, W. Q. Zou, L. Y. Lv, X. C. Liu, S. D. Li, J. M. Zhu, F. M. Zhang, Y. W. Du, J Phys Chem B 2006, 110, 23817; Z. L. Lu, M. X. Xu, W. Q. Zou, S. Wang, X. C. Liu, Y. B. Lin, J. P. Xu, Z. H. Lu, J. F. Wang, L. Y. Lv, F. M. Zhang, Y. W. Du, Appl Phys Lett 2007, 91, 102508.

[11]   O. Knop, K. I. G. Reid, Sutarno, Y. Nakagawa, Can J Chemistry 1968, 46, 3463.

[12]   P. Silwal, L. Miao, I. Stern, X. L. Zhou, J. Hu, D. H. Kim, Appl Phys Lett 2012, 100, 032102.

[13]   B. Cui, H. Lin, J. B. Li, X. Li, J. Yang, J. Tao, Adv Funct Mater 2008, 18, 1440.

[14]   J. Yang, J. B. Li, H. Lin, X. Z. Yang, X. G. Tong, G. F. Guo, J Appl Electrochem 2006, 36, 945.

[15]   R. Alcantara, M. Jaraba, P. Lavela, J. L. Tirado, Chem Mater 2002, 14, 2847; J. F. Li, S. L. Xiong, Y. R. Liu, Z. C. Ju, Y. T. Qian, Acs Appl Mater Inter 2013, 5, 981.

[16]   L. F. Hu, L. M. Wu, M. Y. Liao, X. S. Fang, Adv Mater 2011, 23, 1988; P. Silwal, L. D. Miao, J. Hu, L. Spinu, D. H. Kim, D. Talbayev, J Appl Phys 2013, 114, 103704.

[17]   L. F. Hu, L. M. Wu, M. Y. Liao, X. H. Hu, X. S. Fang, Adv Funct Mater 2012, 22, 998.

[18]   H. Jiang, J. Ma, C. Z. Li, Chem Commun 2012, 48, 4465; G. Q. Zhang, H. B. Wu, H. E. Hoster, M. B. Chan-Park, X. W. Lou, Energ Environ Sci 2012, 5, 9453.

[19]   X. X. Zhang, J. M. Hernandez, J. Tejada, R. F. Ziolo, Phys Rev B 1996, 54, 4101.

[20]   G. F. Goya, T. S. Berquo, F. C. Fonseca, M. P. Morales, J Appl Phys 2003, 94, 3520.

[21]   R. K. Zheng, H. W. Gu, B. Xu, X. X. Zhang, J Phys-Condens Mat 2006, 18, 5905.

[22]   S. Verma, H. M. Joshi, T. Jagadale, A. Chawla, R. Chandra, S. Ogale, J Phys Chem C 2008, 112, 15106.

[23]   P. Sheng, B. Abeles, Y. Arie, Phys Rev Lett 1973, 31, 44.

[24]   J. S. Helman, B. Abeles, Phys Rev Lett 1976, 37, 1429.

[25]   D. T. Margulies, F. T. Parker, M. L. Rudee, F. E. Spada, J. N. Chapman, P. R. Aitchison, A. E. Berkowitz, Phys Rev Lett 1997, 79, 5162; A. V. Ramos, J. B. Moussy, M. J. Guittet, A. M. Bataille, M. Gautier-Soyer, M. Viret, C. Gatel, P. Bayle-Guillemaud, E. Snoeck, J Appl Phys 2006, 100, 103902.

[26]   D. Santos-Carballal, A. Roldan, R. Grau-Crespo, N. H. de Leeuw, Phys Rev B 2015, 91, 195106.

[27]   G. Kresse, J. Hafner, Phys Rev B 1993, 47, 558; G. Kresse, J. Furthmuller, Comp Mater Sci 1996, 6, 15.
[28]   P. E. Blochl, Phys Rev B 1994, 50, 17953.
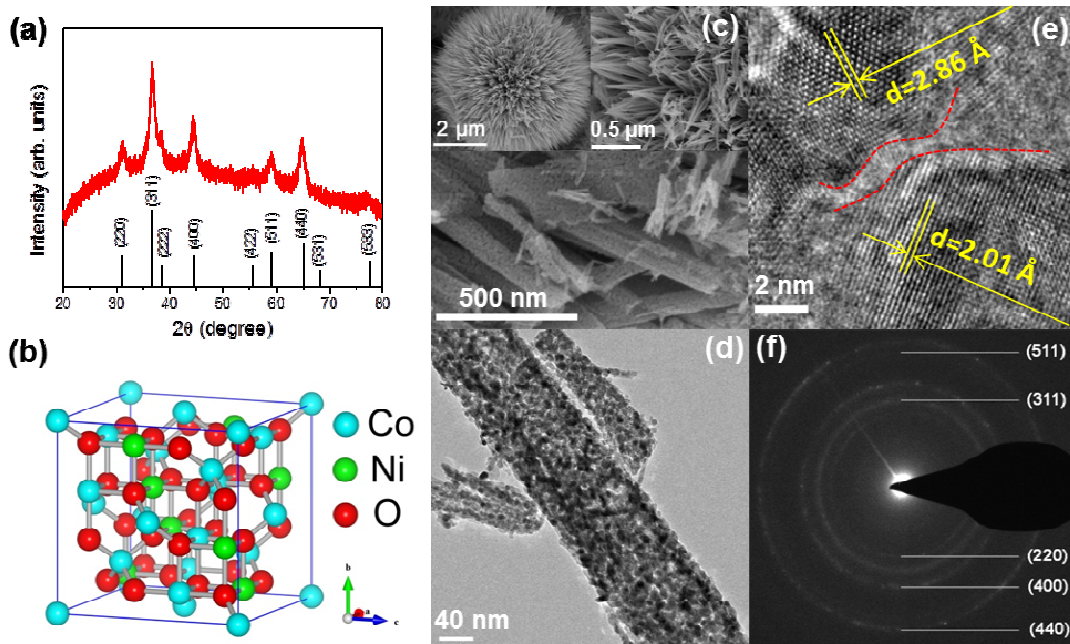[29]   H. J. Monkhorst, J. D. Pack, Phys Rev B 1976, 13, 5188.

Figure 1. a) Typical θ-2θ XRD pattern of NiCo$_2$O$_4$. b) The crystal model of inverse spinel NiCo$_2$O$_4$. c) SEM images of self-assembled urchin-like NiCo$_2$O$_4$. Insets show 3 different scales. d) Typical TEM image of a NiCo$_2$O$_4$ nanotube obtained through an ultrasonic process. e) High resolution TEMR image of NiCo$_2$O$_4$ nanocrystals. f) SAED pattern of NiCo$_2$O$_4$ nanocrystals.
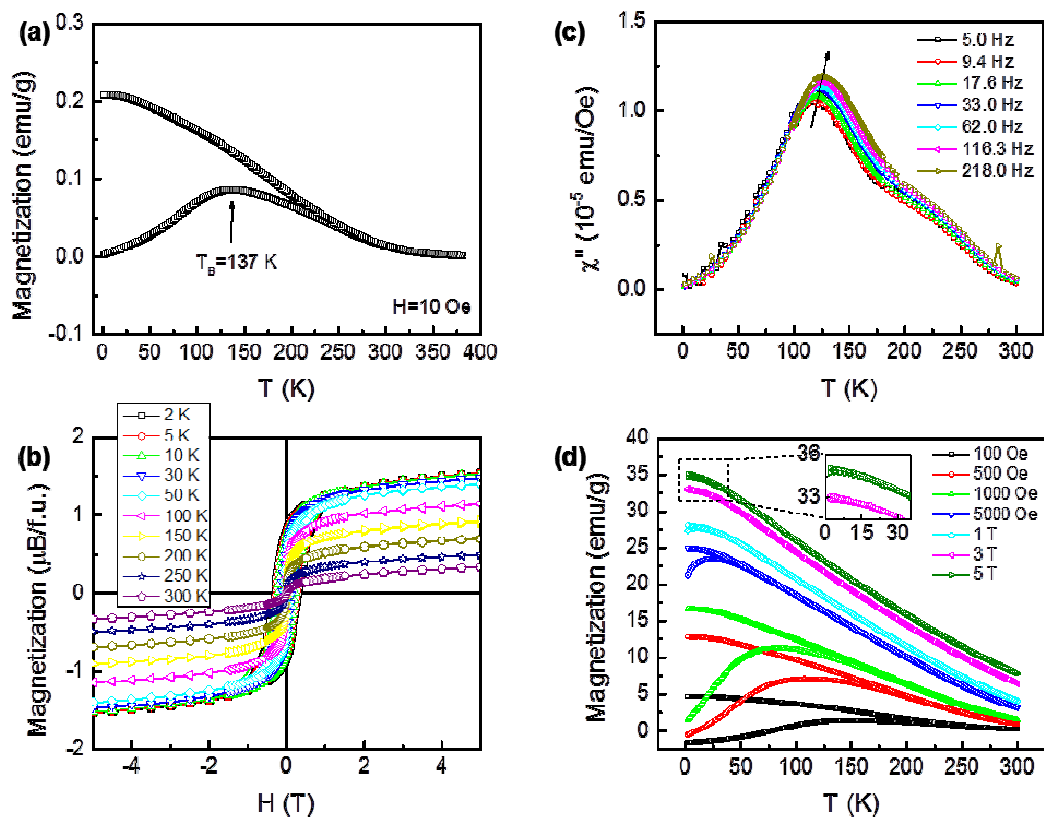
Figure 2. a) $NiCo_2O_4$ temperature dependence of ZFC and FC magnetization at *H*=10 Oe. b)

Hysteresis loops of $NiCo_2O_4$ at different temperatures. c) Temperature dependence of the out-

of-phase (imaginary) part χ'' of the magnetic susceptibility of nanocrystalline $NiCo_2O_4$ at

different frequencies. d) ZFC and FC temperature-dependent magnetization under different
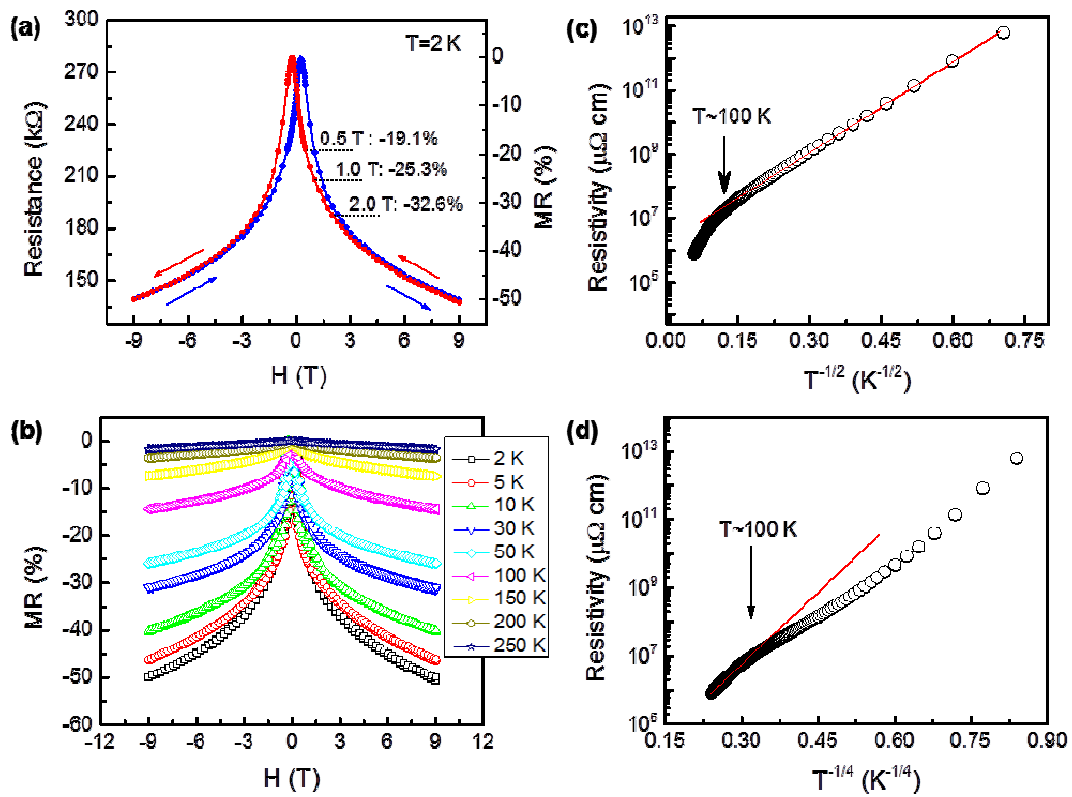
magnetic fields.

Figure 3. a) Resistance and LFMR of NiCo$_2$O$_4$ at 2 K. And the red and blue arrows give the scan direction of magnetic field. b) The MR of NiCo$_2$O$_4$ at different temperatures. c) Plot of resistivity ρ_{xx} of NiCo$_2$O$_4$ versus $T^{-1/2}$. d) Plot of resistivity ρ_{xx} of NiCo$_2$O$_4$ versus $T^{-1/4}$.
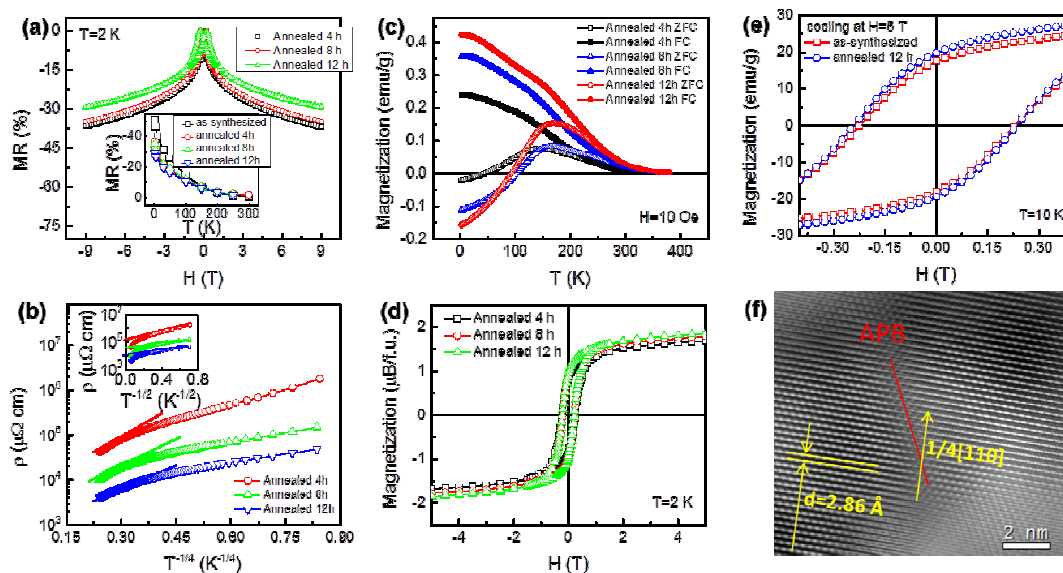
Figure 4. a) Field-dependent MR of $NiCo_2O_4$ for different annealing times. The inset shows the MR ratio (H=9 T) as a function of temperature. b) Plot of resistivity ρ_{xx} of annealed $NiCo_2O_4$ versus $T^{-1/4}$. The inset shows the relation of ρ_{xx} with $T^{-1/2}$. c) Temperature-dependent ZFC and FC magnetization of annealed $NiCo_2O_4$ under a field of 10 Oe. d) The hysteresis loops of $NiCo_2O_4$ with different annealing times at 2 K. e) Comparison of magnetic hysteresis loops of as-synthesized and annealed (12 h) $NiCo_2O_4$, recorded after field-cooling to 2 K with a magnetic field of 5 T. f) Typical HRTEM image of annealed $NiCo_2O_4$ with an antiphase boundary.
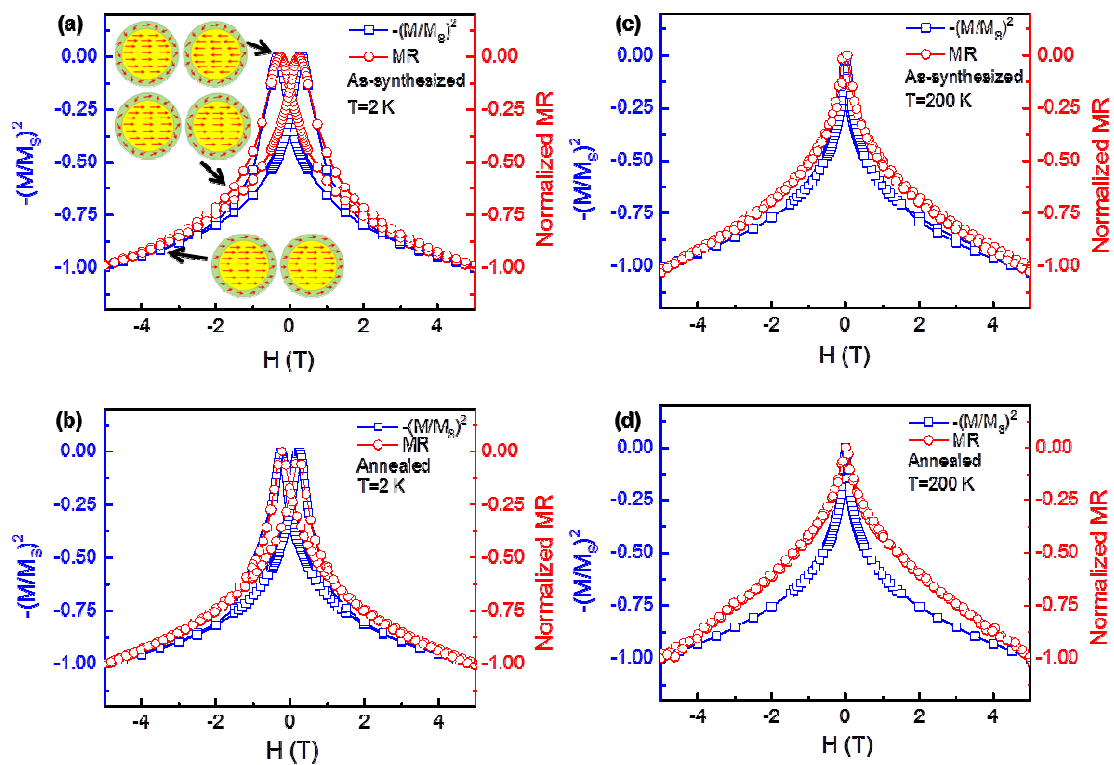
Figure 5. Comparison of normalized MR and $-(M/M_s)^2$ of as-synthesized and annealed NiCo$_2$O$_4$ at different temperatures: a) 2 K, as-synthesized, b) 2 K, annealed, c) 200 K, as-synthesized and d) 200 K, annealed.
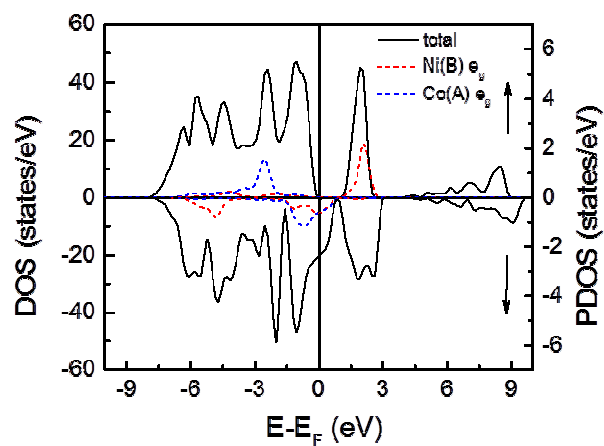
Figure 6. Calculated density of states of NiCo$_2$O$_4$ (solid line) and partial density of states of Co and Ni (red and blue dashed line).

A large low field magnetoresistance of -20% at 0.5 T and a MR of -50% at 9 T are observed in self-assembly nanocrystalline NiCo$_2$O$_4$, which is a non-perovskite-type based system. This work demonstrates the feasibility of spinel oxide half metal in spintronics and opens another door for the family of low field magnetoresistance materials.

Keyword: spinel oxide, low field magnetoresistance, nanocrystalline, half metal

Peng Li[1†]*, Chuan Xia[2†], Dongxing Zheng[1], Ping Wang,[1] Chao Jin[1], and Haili Bai[1]

Observation of Large Low-Field Magnetoresistance in Spinel Cobaltite: A New Half-Metal